Hyperfine Interact (2017) 238:53
DOI 10.1007/s10751-017-1426-6

Preparation and characterization of Fe_3O_4-Pt nanoparticles

Ângela Leão Andrade[1] · Luis Carlos Duarte Cavalcante[2,3] · José Domingos Fabris[3,4] · Márcio César Pereira[5] · José Domingos Ardisson[6] · Rosana Zacarias Domingues[3]

Abstract Pt and Pt-based nanomaterials are active anticancer drugs for their ability to inhibit the division of living cells. Nanoparticles of magnetite containing variable proportions of platinum were prepared in the laboratory. The magnetite nanoparticles with platinum (Pt-Fe_3O_4) were obtained by reducing the Fe^{3+} of the maghemite (γFe_2O_3) mixed with platinum (II) acetylacetonate and sucrose in two inversely coupled ceramic crucibles and heated in a furnace at 400 °C for 20 min. The formed carbon during this preparation acts to chemically reduce the ferric iron in maghemite. Moreover, its residual layer on the

This article is part of the Topical Collection on *Proceedings of the 15th Latin American Conference on the Applications of the Mössbauer Effect (LACAME 2016), 13–18 November 2016, Panama City, Panama*
Edited by Juan A. Jaén

✉ Ângela Leão Andrade
angelala01@hotmail.com

[1] Department of Chemistry, ICEB, Federal University of Ouro Preto (UFOP), 35400-000 Ouro Preto, Minas Gerais, Brazil

[2] Center of Natural Sciences, Federal University of Piauí (UFPI), 64049-550 Teresina, Piauí, Brazil

[3] Department of Chemistry, ICEx, Federal University of Minas Gerais (UFMG), 31270-901 Belo Horizonte, Minas Gerais, Brazil

[4] Federal University of the Jequitinhonha and Mucuri Valleys (UFVJM), 39100-000 Diamantina, Minas Gerais, Brazil

[5] Institute of Science, Engineering and Technology, Federal University of the Jequitinhonha and Mucuri Valleys (UFVJM), 39803-371 Teófilo Otoni, Minas Gerais, Brazil

[6] Laboratory of Applied Physics, Center for the Development of the Nuclear Technology (CDTN), 31270-901 Belo Horizonte, Minas Gerais, Brazil

Published online: 01 May 2017

particle surface prevents the forming magnetite from oxidizing in air and helps retain the platinum in the solid mixture. The produced Pt-magnetite samples were characterized by ^{57}Fe-Mössbauer spectroscopy, powder X-ray diffraction, scanning electron microscopy, and magnetization measurements. Measurements of AC magnetic-field-induced heating properties of the obtained nanocomposites, in aqueous solution, showed that they are suitable as a hyperthermia agent for biological applications.

Keywords Hyperthermia · Medical technology · Oncology · Iron oxide · Magnetization

1 Introduction

Magnetite nanoparticles (MNPs) have been widely considered for the development of some technological materials destined to applications in magnetic resonance imaging (MRI) for clinical diagnosis, magnetic drug targeting, hyperthermia anti-cancer strategy, and enzyme immobilization [1–8]. Magnetite, a commonly found magnetic iron oxide in nature, has a cubic inverse spinel structure with oxygen forming a FCC closed packing, with Fe cations occupying the interstitial tetrahedral and octahedral sites [9]. The electrons can hop between Fe^{2+} and Fe^{3+} ions in octahedral sites at room temperature, conferring to the magnetite an important half-metallic character [10].

Pt and Pt-based nanomaterials are employed as anticancer drugs due their ability to inhibit the division of living cells. The use of nanoscale drug carrier for biomedical applications has several advantages over drugs based on small molecules. These advantages include their lower toxicity, increased accumulation in the target tissue, and a surface functionalization capacity with targeting and passivating moieties [11, 12].

Platinum is inert and does not corrode inside the human body. This property has also favored the development of Pt-based nanomaterials for biomedical applications. Platinum is a transition metal with a partially filled 5d shell. In the form of a bulk metal, Pt shows no evidence of surface magnetism but investigating the magnetic properties of Pt and Pt-based nanomaterials has garnered great interest due to its technological potential for applications in magnetic storage media [13–16].

Over the past decade, several chemical pathways have been developed to synthesize FePt NPs with controlled stoichiometry, size, and shape [17]. Such synthetic routes include co-reduction of Fe and Pt precursors through both low temperature emulsion protocols and the high-temperature polyol pathway [18–20], along with the thermal decomposition route [21–23]. The latter approach often relies on $Pt(acac)_2$, $Fe(CO)_5$, or Collman's reagent precursors mixed with alkyl amines and acids both solubilized in high-boiling-point solvents heated at temperatures of ∼300 °C or above, to control the growth, chemical composition, and morphology of the NPs. More specifically, Pt-containing nanosized magnetic iron oxides have been used in several catalytic processes. Examples are Pt-Fe_3O_4 for oxygen reduction reaction [24] and bimetallic nanoparticles of PtM (M = Au, Cu, Ni) supported on γFe_2O_3, for the radiolytic synthesis and CO oxidation catalysis [25].

Studies have demonstrated the biomedical potential of FePt NPs in magnetic separation [26, 27] and hyperthermic ablation [28, 29] and as T_2 MRI (magnetic resonance imagery) contrast agents [30–32].

It is reported the synthesis and characterization of a family of magnetite-platinum composites NPs, with controlled platinum contents.

2 Materials and methods

2.1 Reagents

All chemicals used in this work, namely a magnetic iron (III) oxide (γFe_2O_3; maghemite) <50 nm particle size (Sigma-Aldrich # 544884-25), sucrose (Synth) and platinum (II) acetylacetonate, $Pt(acac)_2$ (Aldrich) were of analytical grade standards and used as received.

2.2 Synthesis of magnetite and platinum-magnetite

The magnetite-platinum composites were obtained by reduction of the precursor commercial iron (III) oxide and $Pt(acac)_2$ through charcoal product devolatilization at 400 °C. This temperature was determined by differential thermal analysis of the powder commercial iron (III) oxide. Magnetite powders (sample labeled "MtS") was obtained by the same route, without $Pt(acac)_2$.

The synthesis procedure followed to prepare these iron oxide spinels, pure and Pt-containing magnetite samples, was described in more details in ref. [28]. In this work, 1 g of commercial iron (III) oxide was mixed with 5 g of powdered sucrose. This mixture was put into two inversely coupled ceramic crucibles, heated from 20 °C at 10 °C min^{-1} up to 400 °C and held at this temperature for a total heating period of 20 min. For the platinum containing samples, 1 g of commercial iron (III) oxide was mixed with a predefined amount of $Pt(acac)_2$, and 5 g of powdered sucrose. This mixture was submitted to the same heating procedure as for the samples without platinum.

At this temperature, the charcoal particles experimented a severe devolatilization, to produce solid coke, tar, and light gases [33]:

$$\text{Sucrose} \rightarrow \text{charcoal} + \text{tar} + \text{gases } (H_2, CO...) \quad (1)$$

It has been shown that maghemite (γFe_2O_3) undergoes stepwise reduction by CO, which are represented by (2) [33]:

$$3Fe_2O_3 + CO \rightarrow 2Fe_3O_4 + CO_2 \quad (2)$$

The chemical reduction of $Pt(acac)_2$ can be represented by (3)

$$Pt(acac)_2 + CO \rightarrow Pt + CO_2 \quad (3)$$

The amount of $Pt(acac)_2$ in the mixture was planned to contain 5, 10, 20, and 40 mass% Pt: the subsequent powders were labeled "MtS-Pt5", "MtS-Pt10", "MtS-Pt20", and "MtS-Pt40", respectively.

2.3 Characterization techniques

A scanning electron microscope (SEM, Quanta FEG 3D FEI) analysis reveals information about the morphology of the nanoparticles, their size and aggregation. Prior to analysis, the samples were fastened to a sample holder with a double carbon ribbon and covered with a thin gold layer. Information about the crystallographic phase of the samples was determined by powder X-ray diffraction (XRD analysis) measurements, using a Shimadzu XRD 6000 diffractometer equipped with an iron tube (40 kV and 30 mA) and a graphite monochromator. The scans were done between 15 and 70° 2 θ with a scanning speed of 1° 2θ/min. Phases were identified by comparing the experimental X-ray patterns with stan-

dard files compiled by the International Centre for Diffraction Data. Silicon was used as an internal standard. The Rietveld structural refinement from the powder X-ray diffraction data was performed with FULLPROF 2010™ program. The averaged particle size (taken as the dimension of the mean coherent length) was determined from the XRD data using the Scherrer formula [34] for the reflection peak breadth at half-height corresponding to the plane (311) of the spinel structure [35], for each sample. The Mössbauer spectra were collected with a constant acceleration transmission mode setup, with a ∼50 mCi ^{57}Co/Rh gamma-ray source. Spectra at 298 K were obtained with a spectrometer equipped with a transducer (CMTE model MA250) controlled by a linear function driving (CMTE model MR351). Values of Mössbauer isomer shifts are quoted relatively to the α-Fe foil. The experimental reflections were fitted to Lorentzian functions by least-square fitting with software NORMOS-90™ (developed by R. A. Brand, at Laboratorium für Angewandte Physik, Universität Duisburg, D-47048, Duisburg-Germany). The magnetization measurements were made at room temperature (RT) on a LakeShore vibrating sample magnetometer (VSM).

Heat dissipation experiments were carried out by transferring the suspensions with the dispersed nanoparticles of iron oxide spinels in water into a test tube. A three-loop coil (Nova Star 5kW RF Power Supply, Ameritherm, Inc) with resonant frequency of 198 kHz was used in the experiments, allowing to correlate the applied magnetic field and the AC magnetically induced heating temperature. The sample concentration was approximately 10 mg g^{-1}. The temperature of the magnetic suspension was measured with an optical fiber thermometer. Results were taken as the mean of triplicate measurements. The amount of heat generated by pure water in the two AC magnetic fields was measured, to obtain any contribution of water to rise the temperature by dispersing the nanoparticles. The whole contribution of pure water was discounted from the final temperature value for each ferrofluid.

3 Results and discussion

3.1 Characterization of the iron (III) oxide commercial

To investigate in more details the conversion of maghemite into magnetite, the Mössbauer measurements were carried out with the sample commercial iron (III) oxide at 298 K. The collected spectrum is shown in Fig. 1 and the hyperfine parameters obtained from the fitting these spectra are summarized in Table 1. Two sites were assigned to maghemite: (i) $\delta = 0.33$ mm s^{-1} and $B_{hf} = 50.3$ T, with $RA = 77\%$, due to the octahedral coordination site, and (ii) $\delta = 0.30$ mm s^{-1} and $B_{hf} = 48.8$ T, with $RA = 13\%$, due to the tetrahedral coordination site of the spinel structure. A third site with $\delta = 0.46$ mm s^{-1} and $B_{hf} = 43.5$ T, with $RA = 10\%$ is assumed to be due to a fraction of the sample of small particles of maghemite experiencing collective magnetic excitation, which reduces the hyperfine field, relatively to that of the bulk material [36, 37].

3.2 Characterization of the synthesized iron oxide

XRD results (Fig. 2) showed essentially the occurrence a single crystallographic phase of magnetite with cubic lattice parameters $a = 8.3961(4)$ Å along with a minor proportion of hematite. The peaks on the XRD patterns match well the corresponding data for magnetite of the powder diffraction file (PDF) from International Centre for Diffraction Data (ICDD) (cards # 019-0629 and # 033-0664 for magnetite and hematite, respectively).

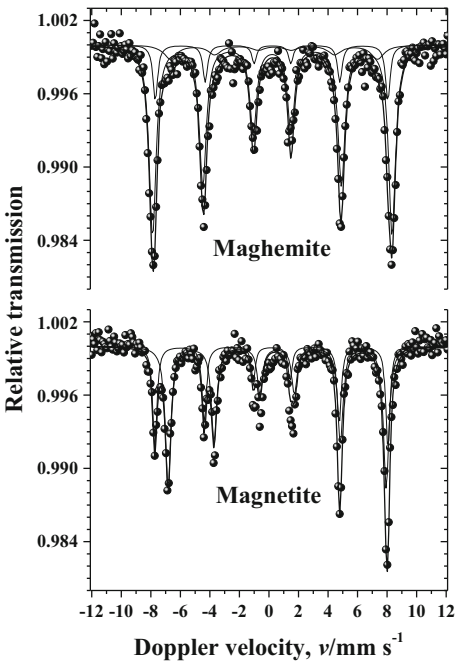

Fig. 1 298 K-Mössbauer spectra for the commercial iron (III) oxide (*upper figure*) and for the produced magnetite (MtS; *botttom*), obtained from calcining the ferric oxide with sucrose

Table 1 Hyperfine parameters of the fitted Mössbauer spectra for the commercial iron (III) oxide and for the magnetite obtained recorded at 298 K

δ = isomer shift relative to αFe; 2ε = quadrupole shift; B_{hf} = magnetic hyperfine field; RA = relative subspectral area

Sample	δ/mm s^{-1}	2ε/mm s^{-1}	B_{hf}/T	RA/%
Maghemite	0.33	0.01	50.3	77
	0.30	−0.06	48.8	13
	0.46	−0.04	43.5	10
Magnetite	0.65	0.04	45.9	64
	0.27	−0.02	48.9	34

The Mössbauer spectrum for sample MtS at 298 K (Fig. 1; corresponding hyperfine parameters, in Table 1) consists of two sextets, one assignable to high spin Fe^{3+} on tetrahedral sites (B_{hf} = 48.9 T) and the other to mixed valence $Fe^{3+/2+}$ on octahedral sites (B_{hf} = 45.9 T) of the magnetite structure. Electron delocalization causes the nucleus to sense an averaged valence $Fe^{3+/2+}$. Considering that the recoilless fraction of octahedral sites at room temperature is 6% less than that of the tetrahedral site [38] the relative area ratio RA_{oct}/RA_{tet} = 1.88 indicates that the magnetite obtained by sucrose reduction is close to its pure stoichiometric form.

From the medical applications point of view, the superparamagnetic relaxation and the high saturation magnetization (M_s) are the two important features of the magnetite nanoparticles. It was measured the magnetization hysteresis curve for the obtained Fe_3O_4 nanoparticles (sample MtS; Fig. 3), by using a vibrating sample magnetometer (VSM) at room temperature. The curve indicates a superparamagnetic behavior of the sample, as evidenced by the values of remnant magnetization and the coercivity clearly approach zero (please, refer to the inset of Fig. 3). It might be useful to remind that the characteristic time-window relies on the method used to measure the superparamagnetic relaxation time. For

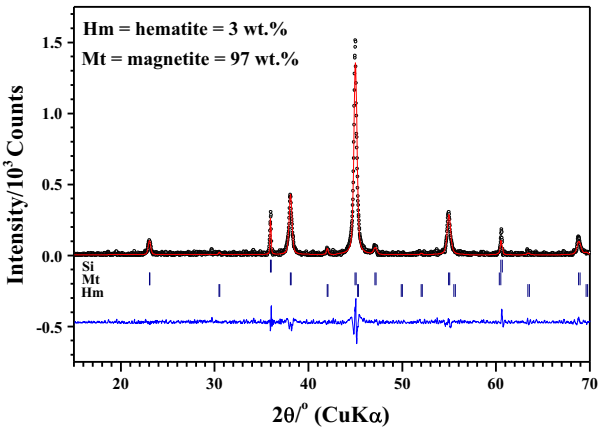

Fig. 2 X-ray diffraction pattern for the obtained magnetite (sample MtS)

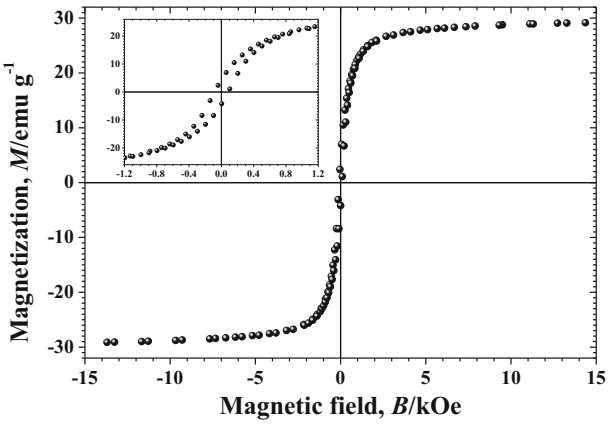

Fig. 3 VSM magnetization curve for the MtS sample. Inset: a scale expansion to show a non-null coercivity

magnetic measurements, it is reported to be ∼10 s, for magnetic susceptibility [39], and ∼100 s, for magnetization [40]; for Mössbauer spectroscopy, it is the mean lifetime (τ) of the 14.4 keV level of the ^{57}Fe gamma cascade: taking into account the half-life $t_{\frac{1}{2}} = 98.1$ ns [41], the time-window is equivalent to $\tau = \frac{t_{\frac{1}{2}}}{\ln 2} = 141.5$ ns. The reported value in ref. [42] is $\tau = 140$ ns.

The saturation magnetization (M_S) was obtained from the magnetic moment curves as a function of the magnetic field (B) applied. For the magnetite MtS sample, the saturation magnetization value was found to be 29.4 emu g^{-1}. This value is much lower than that expected for the bulk material ($M_S \sim 93$ emu g^{-1}). The decrease in the value of M_S of the nanoparticles is due to the effect of the small size and surface effects [43–47]. Moreover, the sample is coated with an organic coating, which also contributes to the lower the specific magnetization [48].

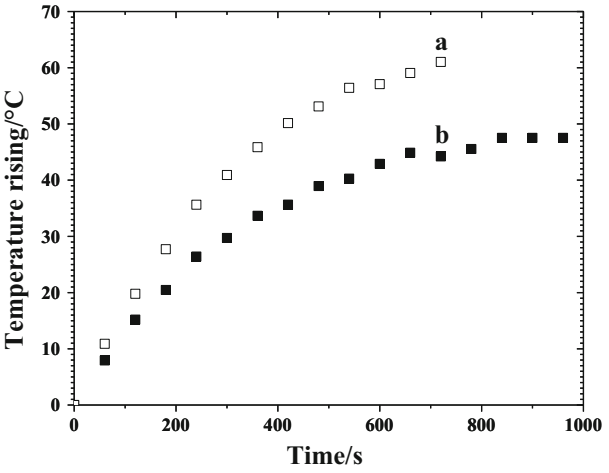

Fig. 4 Temperature-time curve for the sample MtS, in water at: **a** 168 Oe, and **b** 105 Oe

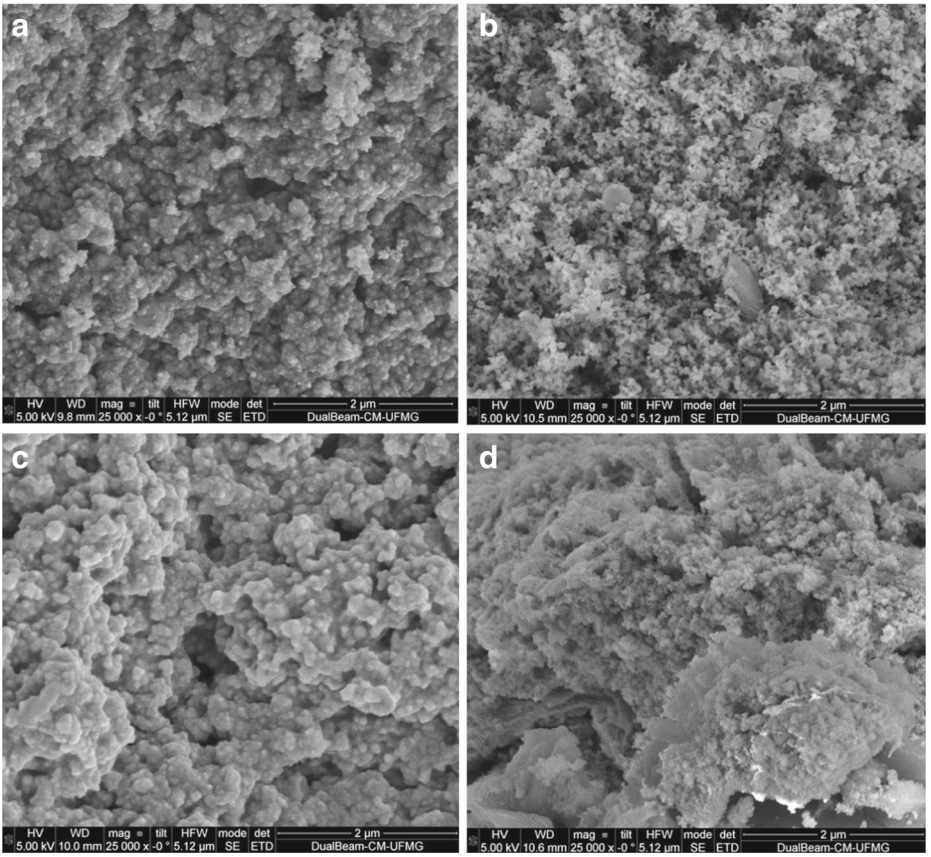

Fig. 5 SEM micrographs of the samples: **a** MtS-Pt5, **b** MtS-Pt10, **c** MtS-Pt20 and **d** MtS-Pt40

Table 2 Averaged values for mass%, cubic lattice parameters and mean crystallite size (actually, mean coherent length) as determined from X-ray diffraction data for this solid solution of iron oxide spinels

Sample	Partially oxidized magnetite			Platinum metal		
	Mass%	a/Å	Mean lengths/nm	Mass%	a/Å	Mean lengths/nm
MtS-Pt5	94	8.3857(7)	34(2)	6	3.909(6)	5(1)
MtS-Pt10	89	8.3870(6)	35(2)	11	3.903(3)	5(1)
MtS-Pt20	74	8.3808(7)	35(2)	26	3.905(1)	5(1)
MtS-Pt40	55	8.3820(8)	38(2)	45	3.910(1)	5(1)

a = Cubic unit cell dimension

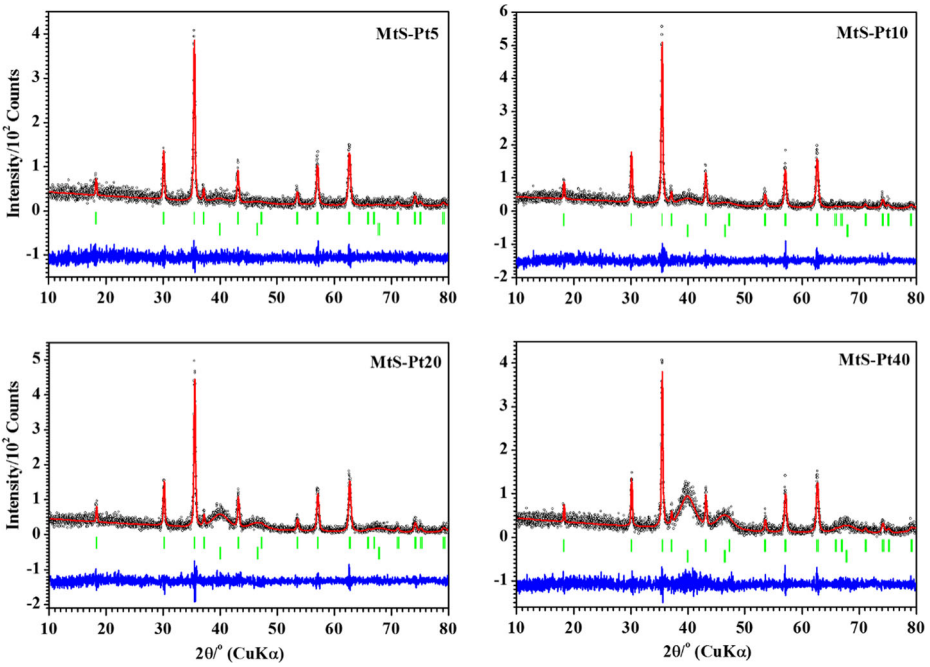

Fig. 6 X-ray diffraction patterns for the MtS-Pt5, MtS-Pt10, MtS-Pt20 and MtS-Pt40 samples

Figure 4 is the hyperthermic ability of MtS samples, at a concentration of 10 mg g^{-1} under magnetic fields of 168 (Fig. 4a) and 105 Oe (Fig. 4b) at a fixed frequency of 198 kHz for 12 and 16 min, respectively, in water. It was observed that the time required, ∼10 min, to reach the plateau of the maximum hyperthermic temperature decreased with increasing magnetic field. This decrease in the heating rate is due to the thermal effect that degradates the magnetic particles [49]. The physical nature of the rapid temperature increase in the initial stages can be attributed to loss processes. There are at least three different mechanisms by which a magnetic material can generate heat in an oscillating field [50]: (i) movement of eddy currents induced in the material, (ii) loss of energy by hysteresis of multi-domain materials and (iii) loss energy for relaxation in mono-domains of superparamagnetic materials. The mechanisms (i) and (ii) contribute very few to heating. The most

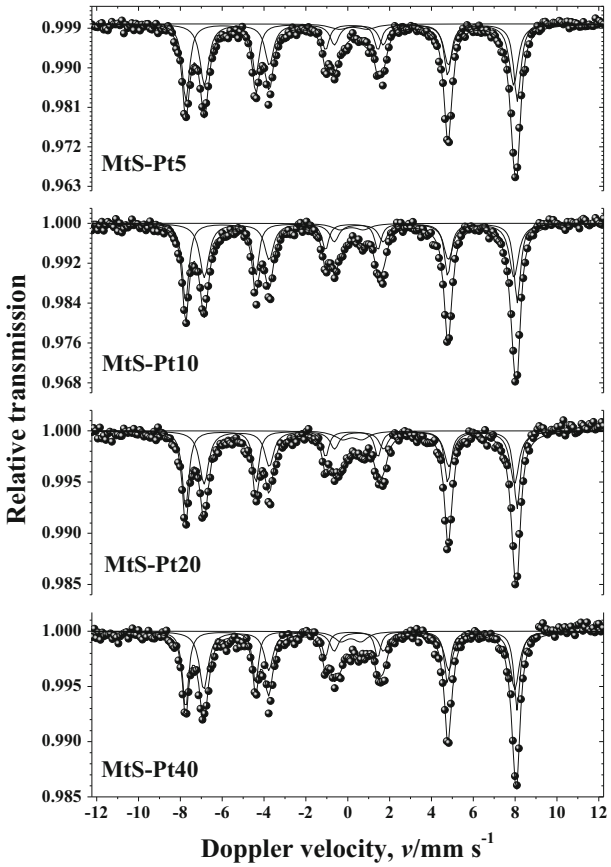

Fig. 7 298 K-Mössbauer spectra for the samples MtS-Pt5, MtS-Pt10, MtS-Pt20, and MtS-Pt40

significant mechanism contributing to heating of these particles as the relaxation mechanisms (iii), which can occur in two ways: rotationally (Brown) and Néel modes. In this case, both samples show relaxation behaviors driving the heat generation, and therefore, the Brownian motion and the Néel mechanism respond for the heat generation.

The value of the maximum temperature (T_{max}) for the MtS sample increased from 45 to 62 °C, if the field is increased from 105 to 168 Oe at 198 kHz. This small increase in temperature if the field is increased can be explained by the carbon coating, which might be inhibiting the Brownian motion. The value of T_{max} for the two samples indicates that they can be considered for hyperthermia for *in vivo* applications. Typically, the temperature of 42–44 °C is regarded as effective to be applicable in medical hyperthermia therapies.

3.3 Characterization of the synthesized Pt-Fe_3O_4 nanoparticles

Figure 5 shows the SEM micrographs of the four samples. The SEM micrographs of MtS-Pt5, MtS-Pt10, MtS-Pt20 and MtS-Pt40 samples show reasonably comparable morphologies of nanoparticles with some agglomeration.

Table 3 Parameters from fitting ^{57}Fe Mössbauer spectra recorded at 298 K

Sample	Fe site	δ/mm s^{-1}	2ε, Δ/mm s^{-1}	B_{hf}/T	RA/%
MtS-Pt5	Magnetite	0.29(1)	−0.00(1)	49.13(2)	41.2(1)
		0.64(1)	0.01(1)	45.84(2)	51.0(1)
	Fe^{3+}	0.35(4)	1.36(7)		7.8(1)
MtS-Pt10	Magnetite	0.28(1)	−0.01(1)	49.16(2)	38.9(1)
		0.63(1)	0.02(1)	45.90(3)	53.3(1)
	Fe^{3+}	0.29(1)	1.13(6)		7.8(1)
MtS-Pt20	Magnetite	0.28(1)	−0.02(1)	49.13(3)	38.3(1)
		0.65(1)	0.01(1)	46.01(3)	51.8(1)
	Fe^{3+}	0.31(3)	0.94(5)		9.9(1)
MtS-Pt40	Magnetite	0.28(1)	−0.01(1)	49.13(3)	33.6(1)
		0.64(1)	0.03(1)	46.09(4)	55.9(1)
	Fe^{3+}	0.25(4)	0.96(6)		10.5(1)

δ = isomer shift relative to αFe; 2ε = quadrupole shift; Δ = quadrupole splitting; B_{hf} = magnetic hyperfine field; RA = relative subspectral area. The number in parentheses are uncertainties over the last significant digit, as it was estimated from the least-squares fitting algorithm

The Table 2 shows the averaged mass% Pt, along with values of cubic lattice parameters and mean crystallite size (actually, the mean coherent length) for the samples MtS-Pt5, MtS-Pt10, MtS-Pt20, and MtS-Pt40, as determined from X-ray diffraction data. The corresponding powder X-ray patterns are presented in Fig. 6.

The 298 K-Mössbauer spectra collected for the nanoparticles of magnetite-metallic platinum, as obtained by chemically reducing the maghemite with sucrose mixed with 5, 10, 20 and 40 mass% of platinum are show in Fig. 7. The corresponding fitted Mössbauer parameters are presented in the Table 3. A central doublet corresponding to a relative subspectral area $RA \lesssim 10\%$ appears in all spectra. Although no further experimental attempt to get more information about any phase change, this may be immediately interpreted as being due to either any paramagnetic phase from side chemical reaction during the sample preparation or superparamagnetic iron oxide of small particle sizes. To better clarify this point, future Mössbauer measurements are to be made with the sample at lower temperatures.

Figure 8 shows the magnetization curves of the MtS-Pt10, MtS-Pt20 and MtS-Pt40 samples. The saturation magnetization, M_s, varies between ∼20 emu g^{-1} and ∼24 emu g^{-1}, which is somewhat lower than that found for the MtS sample, 29.4 emu g^{-1}.

Figure 9 shows the variation of the hyperthermic heat with time for assays performed with different samples. These results were given in relation to the concentration of magnetite in each sample, as obtained by analyzing the powder X-ray patterns. Differences of the maximum temperatures, $\Delta T_{max} = T_{final} - T_{initial}$, for samples MtS-Pt5, MtS-Pt10, MtS-Pt20 and MtS-Pt40 were found to be nearly 10, 16, 11 and 22 °C, respectively. It is interesting to mention that the ΔT_{max} varies systematically with the proportion of platinum in the Pt-magnetite samples, but this trend, although not strictly, roughly follows the inverse sequence observed for the values of saturation magnetization (Fig. 8). According to the reported from the scientific literature, the heat generation corresponding to a temperature rising between 4.5 and 7.5 °C, so that the local body temperature rises from 35.5 to 41 °C and 43 °C, is sufficient for uses in the treatment by hyperthermia. Therefore, all these samples are materials potentially interesting for further development intending to be used in medical

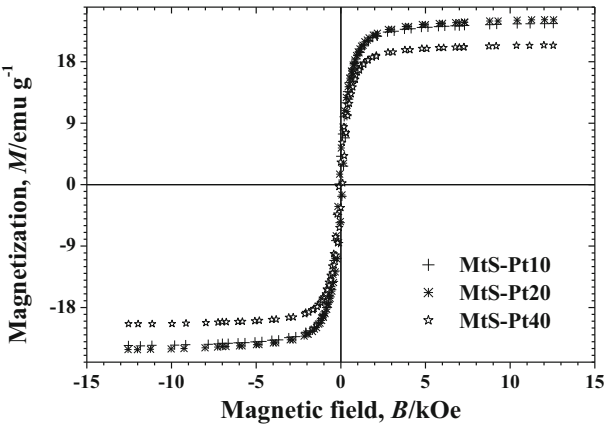

Fig. 8 VSM magnetization curves for the MtS-Pt10, MtS-Pt20 and MtS-Pt40 samples

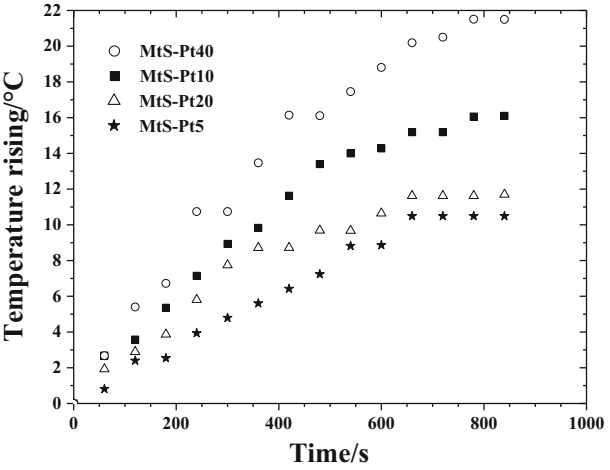

Fig. 9 Temperature-time curves of the samples: MtS-Pt5, MtS-Pt10, MtS-Pt20, and MtS-Pt40, in water at 168 Oe

practices. Other assays with living cells will be next performed in order to evaluate the real hyperthermic effect for such an application.

4 Conclusions

Magnetite was directly and promptly synthesized by mixing a ferric iron oxide (in this case, maghemite) precursor, with sucrose and platinum (II) acetylacetonate, followed by treating the mixture at 400 °C for 20 min. As far as their hyperthermic behavior is concerned, the produced materials were found to be indeed suitable for still further technological development towards their application in medical practices. Moreover, this simple and direct method to produce such hyperthermic materials may be thinkable as a facile route to render resources

in complex medical therapies, particularly in oncology, for two main combined effects: their magnetic hyperthermic heating and the healing action of platinum in malignant tumors.

Acknowledgements Work supported by FAPEMIG (Brazil; grants # CEX-PPM-00412-15, PEE-01481-16 and APQ-00651-11). JDF is indebted to CAPES (Brazil) for granting his Visiting Professorship at UFVJM under the PVNS program and to CNPq for the grant # 305755-2013-7.

References

1. Kim, D.K., Zhang, Y., Kehr, J., Klason, T., Bjelke, B., Muhammed, M.: Characterization and MRI study of surfactant-coated superparamagnetic nanoparticles administered into the rat brain. J. Magn. Magn. Mater. **225**(1–2), 256–261 (2001). doi:10.1016/S0304-8853(00)01255-5
2. Reynolds, C.H., Annan, N., Beshah, K., Huber, J.H., Shaber, S.H., Lenkinski, R.E., Wortman, J.A.: Gadolinium-loaded nanoparticles: new contrast agents for magnetic resonance imaging. J. Am. Chem. Soc. **122**(37), 8940–8945 (2000). doi:10.1021/ja001426g
3. Andrade, A.L., Fabris, J.D., Domingues, R.Z., Pereira, M.C.: Current status of magnetite-based core@shell structures for diagnosis and therapy in oncology. Curr. Pharm. Des. **21**(37), 5417–5433 (2015). doi:10.2174/1381612821666150917093543
4. Bergemann, C., Müller-Schulte, D., Oster, J., à Brassard, L., Lübbe, A.S.: Magnetic ion-exchange nano- and microparticles for medical, biochemical and molecular biological applications. J. Magn. Magn. Mater. **194**(1-3), 45–52 (1999). doi:10.1016/S0304-8853(98)00554-X
5. Andrade, A.L., Valente, M.A., Ferreira, J.M.F., Fabris, J.D.: Preparation of size-controlled nanoparticles of magnetite. J. Magn. Magn. Mater. **324**(10), 1753–1757 (2012). doi:10.1016/j.jmmm.2011.12.033
6. Jordan, A., Scholz, R., Wust, P., Schirra, H., Schiestel, T., Schmidt, H., Felix, R.: Endocytosis of dextran and silan-coated magnetite nanoparticles and the effect of intracellular hyperthermia on human mammary carcinoma cells in vitro. J. Magn. Magn. Mater. **194**(1–3), 185–196 (1999). doi:10.1016/S0304-8853(98)00558-7
7. Dyal, A., Loos, K., Noto, M., Chang, S.W., Spagnoli, C., Shafi, K.V.P.M., Ulman, A., Cowman, M., Gross, R.A.: Activity of *Candida rugosa* lipase immobilized on γ-Fe_2O_3 magnetic nanoparticles. J. Am. Chem. Soc. **125**(7), 1684–1685 (2003). doi:10.1021/ja021223n
8. Andrade, A.L., Fabris, J.D., Pereira, M.C., Domingues, R.Z., Ardisson, J.D.: Preparation of composite with silica-coated nanoparticles of iron oxide spinels for applications based on magnetically induced hyperthermia. Hyperfine Interact. **218**(1–3), 71–82 (2013). doi:10.1007/s10751-012-0681-9
9. Cornell, R.M., Schwertmann, U.: The Iron Oxides: Structure, Properties, Reactions, Occurrence and Uses, pp. 28–29. VCH, New York (1996)
10. Verwey, E.J.W.: Electronic conduction of magnetite (Fe_3O_4) and its transition point at low temperatures. Nature **144**(3642), 327–328 (1939). doi:10.1038/144327b0
11. Gao, J.H., Liang, G.L., Zhang, B., Kuang, Y., Zhang, X.X., Xu, B.: FePt@CoS2 yolk-shell nanocrystals as a potent agent to kill HeLa cells. J. Am. Chem. Soc. **129**(5), 1428–1433 (2007). doi:10.1021/ja067785e
12. Rieter, W.J., Pott, K.M., Taylor, K.M.L., Lin, W.B.: Nanoscale coordination polymers for platinum-based anticancer drug delivery. J. Am. Chem. Soc. **130**(35), 11584–11585 (2008). doi:10.1021/ja803383k
13. Petit, C., Rusponi, S., Brune, H.: Magnetic properties of cobalt and cobalt-platinum nanocrystals investigated by magneto-optical Kerr effect. J. Appl. Phys. **95**(8), 4251–4260 (2004). doi:10.1063/1.1686906
14. Delin, A., Tosatti, E.: Emerging magnetism in platinum nanowires. Surf. Sci. **566**, 262–267 (2004). doi:10.1016/j.susc.2004.05.055
15. Liu, X., Bauer, M., Bertagnolli, H., Roduner, E., van Slageren, J., Phillipp, F.: Structure and magnetization of small monodisperse platinum clusters. Phys. Rev. Lett. **97**(25), 253401 (2006). doi:10.1103/PhysRevLett.97.253401
16. Yang, X.M., Liu, C., Ahner, J., Yu, J., Klemmer, T., Johns, E., Weller, D.: Fabrication of FePt nanoparticles for self-organized magnetic array. J. Vac. Sci. Technol. B **22**(1), 31–34 (2004). doi:10.1116/1.1633283
17. Pankhurst, Q.A., Connolly, J., Jones, S.K., Dobson, J.: Applications of magnetic nanoparticles in biomedicine. J. Phys. D: Appl. Phys. **36**(13), R167–R181 (2003). doi:10.1088/0022-3727/36/13/201
18. Nakaya, M., Kanehara, M., Teranishi, T.: One-pot synthesis of large FePt nanoparticles from metal salts and their thermal stability. Langmuir **22**(8), 3485–3487 (2006). doi:10.1021/la053504p

19. Yan, Q.Y., Purkayastha, A., Kim, T., Kroger, R., Bose, A., Ramanath, G.: Synthesis and assembly of monodisperse high-coercivity silica-capped FePt nanomagnets of tunable size, composition, and thermal stability from microemulsions. Adv. Mater. **18**(19), 2569–2573 (2006). doi:10.1002/adma.200502607
20. Saita, S., Maenosono, S.: Formation mechanism of FePt nanoparticles synthesized via pyrolysis of iron(III) ethoxide and platinum(II) acetylacetonate. Chem. Mater. **17**(26), 6624–6634 (2005). doi:10.1021/cm051760h
21. Nandwana, V., Elkins, K.E., Poudyal, N., Chaubey, G.S., Yano, K., Liu, J.P.: Size and shape control of monodisperse FePt nanoparticles. J. Phys. Chem. C **111**(11), 4185–4189 (2007). doi:10.1021/jp068330e
22. Nguyen, H.L., Howard, L.E.M., Stinton, G.W., Giblin, S.R., Tanner, B.K., Terry, I., Hughes, A.K., Ross, I.M., Serres, A., Evans, J.S.O.: Chem. Mater. **18**(26), 6414–6424 (2006). doi:10.1021/cm062127e
23. Delalande, M., Marcoux, P.R., Reiss, P., Samson, Y.: Core-shell structure of chemically synthesised FePt nanoparticles: a comparative study. J. Mater. Chem. **17**(16), 1579–1588 (2007). doi:10.1039/b614209e
24. Yamamoto, T.A., Nakagawa, T., Seino, S., Nitani, H.: Bimetallic nanoparticles of PtM (M = Au, Cu, Ni) supported on iron oxide: radiolytic synthesis and CO oxidation catalysis. Appl. Catal. A: Gen. **387**(1–2), 195–202 (2010). doi:10.1016/j.apcata.2010.08.020
25. Wang, C., Daimon, H., Sun, S.: Dumbbell-like Pt-Fe_3O_4 nanoparticles and their enhanced catalysis for oxygen reduction reaction. Nano Lett. **9**(4), 1493–1496 (2009). doi:10.1021/nl8034724
26. Gu, H.W., Ho, P.L., Tsang, K.W.T., Yu, C.W., Xu, B.: Using biofunctional magnetic nanoparticles to capture Gram-negative bacteria at an ultra-low concentration. Chem. Commun. 1966–1967. doi:10.1039/b305421g (2003)
27. Gu, H.W., Ho, P.L., Tsang, K.W.T., Wang, L., Xu, B.: Using biofunctional magnetic nanoparticles to capture vancomycin-resistant enterococci and other gram-positive bacteria at ultralow concentration. J. Am. Chem. Soc. **125**(51), 15702–15703 (2003). doi:10.1021/ja0359310
28. Paiva, D.L., Andrade, A.L., Pereira, M.C., Fabris, J.D., Domingues, R.Z., Alvarenga, M.E.: Novel protocol for the solid-state synthesis of magnetite for medical practices. Hyperfine Interact. **232**(1), 19–27 (2015). doi:10.1007/s10751-015-1124-1
29. Seehra, M.S., Singh, V., Dutta, P., Neeleshwar, S., Chen, Y.Y., Chen, C.L., Chou, S.W., Chen, C.C.: Size-dependent magnetic parameters of fcc FePt nanoparticles: applications to magnetic hyperthermia. J. Phys. D: Appl. Phys. **43**(14), 145002 (2010). doi:10.1088/0022-3727/43/14/145002
30. Maenosono, S., Suzuki, T., Saita, S.: Superparamagnetic FePt nanoparticles as excellent MRI contrast agents. J. Magn. Magn. Mater. **320**(9), L79–L83 (2008). doi:10.1016/j.jmmm.2008.01.026
31. Gao, J.H., Liang, G.L., Cheung, J.S., Pan, Y., Kuang, Y., Zhao, F., Zhang, B., Zhang, X.X., Wu, E.X., Xu, B.: Multifunctional yolk-shell nanoparticles: a potential MRI contrast and anticancer agent. J. Am. Chem. Soc. **130**(35), 11828–11833 (2008). doi:10.1021/ja803920b
32. Chou, S.W., Shau, Y.H., Wu, P.C., Yang, Y.S., Shieh, D.B., Chen, C.C.: In vitro and in vivo studies of FePt nanoparticles for dual modal CT/MRI molecular imaging. J. Am. Chem. Soc. **132**(38), 13270–13278 (2010). doi:10.1021/ja1035013
33. Cotton, F.A., Wilkinson, G.: Advanced Inorganic Chemistry. Wiley Interscience, New York (1988)
34. Scherrer, P.: Nachr. Ges. Wiss. Gottingen. **26**, 98–100 (1918). *Apud*: Patterson, A.L.: The Scherrer formula for X-ray particle size determination. Phys. Rev. **56**, 978–982 (1939) doi:10.1103/PhysRev.56.978
35. Mahadevan, S., Gnanaprakash, G., Philip, J., Rao, B.P.C., Jayakumar, T.: X-ray diffraction-based characterization of magnetite nanoparticles in presence of goethite and correlation with magnetic properties. Phys. E **39**, 20–25 (2007). doi:10.1016/j.physe.2006.12.041
36. Mørup, S., Topsøe, H., Lipka, J.: Modified theory for Mössbauer spectra of superparamagnetic particles: application to Fe_3O_4. J. Phys. **37**(C6, s12), C6-287–C6-290 (1976). doi:10.1051/jphyscol:1976658
37. Mørup, S., Frandsen, C., Hansen, M.F.: Uniform excitations in magnetic nanoparticles. Beilstein J. Nanotechnol. **1**, 48–54 (2010). doi:10.3762/bjnano.1.6
38. Sawatzky, G.A., Vanderwo, F., Morrish, A.H.: Mössbauer study of several ferrimagnetic spinels. Phys. Rev. **187**(2), 747–757 (1969). doi:10.1103/PhysRev.187.747
39. Rebbouh, L., Hermann, R.P., Grandjean, F., Hyeon, T., An, K., Amato, A., Long, G.J.: ^{57}Fe Mössbauer spectral and muon spin relaxation study of the magnetodynamics of monodispersed $\gamma-Fe_2O_3$ nanoparticles. Phys. Rev. B **76**, 174422 (2007). doi:10.1103/PhysRevB.76.174422
40. Morales, M.A., Rodrigues, E.C.S., de Amorim, A.S.C.M., Soares, J.M., Galembeck, F.: Size selected synthesis of magnetite nanoparticles in chitosan matrix. Appl. Surf. Sci. **275**, 71–74 (2013). doi:10.1016/j.apsusc.2013.01.123
41. Raghavan, P.: Table of nuclear moments. At. Data Nucl. Data Tables **42**(2), 189–291 (1989). *Apud* Mössbauer Effect Reference and Data Journal **25**(1), 2-2 (2002)
42. Gütlich, P., Goodwin, H.A.: Spin Crossover in Transition Metal Compounds II. Topics in Current Chemistry 234, p. 235. Springer, Berlin Heidelberg (2004). doi:10.1007/b93641

43. He, Y.P., Wang, S.Q., Li, C.R., Miao, Y.M., Wu, Z.Y., Zou, B.S.: Synthesis and characterization of functionalized silica-coated Fe_3O_4 superparamagnetic nanocrystals for biological applications. J. Phys. D: Appl. Phys. **38**(9), 1342–1350 (2005). doi:10.1088/0022-3727/38/9/003
44. Iglesias, O., Labarta, A.: Finite-size and surface effects in maghemite nanoparticles: Monte Carlo simulations. Phys. Rev. B **63**(18), 184416 (2001). doi:10.1103/PhysRevB.63.184416
45. Goya, G.F., Berquo, T.S., Fonseca, F.C., Morales, M.P.: Static and dynamic magnetic properties of spherical magnetite nanoparticles. J. Appl. Phys. **94**(5), 3520–3528 (2003). doi:10.1063/1.1599959
46. Woo, K., Hong, J., Choi, S., Lee, H.W., Ahn, J.P., Kim, C.S., Lee, S.W.: Easy synthesis and magnetic properties of iron oxide nanoparticles. Chem. Mater. **16**(14), 2814–2818 (2004). doi:10.1021/cm049552x
47. Saravanan, P., Alam, S., Mathur, G.N.: Comparative study on the synthesis of gamma-Fe_2O_3 and Fe_3O_4 nanocrystals using high-temperature solution-phase technique. J. Mater. Sci. Lett. **22**(18), 1283–1285 (2003). doi:10.1023/A:1025470405000
48. Zhang, L.Y., Gu, H.C., Wang, X.M.: Magnetite ferrofluid with high specific absorption rate for application in hyperthermia. J. Magn. Magn. Mater. **311**(1), 228–233 (2007). doi:10.1016/j.jmmm.2006.11.179
49. Bae, S., Lee, S.W., Takemura, Y., Yamashita, E., Kunisaki, J., Zurn, S., Kim, C.S.: Dependence of frequency and magnetic field on self-heating characteristics of $NiFe_2O_4$ nanoparticles for hyperthermia. IEEE Trans. Magn. **42**(10), 3566–3568 (2006). doi:10.1109/TMAG.2006.879617
50. Kalambur, V.S., Han, B., Hammer, B.E., Shield, T.W.: Bischof, J.C.: In vitro characterization of movement, heating and visualization of magnetic nanoparticles for biomedical applications. Nanotechnol **16**(8), 1221–1233 (2005). doi:10.1088/0957-4484/16/8/041